Recoil Anisotropy following Molecular Predissociation: $NH_3^* \rightarrow H + NH_2$ and $HFCO^* \rightarrow H + FCO$

Richard N. Dixon* and Thomas W. R. Hancock

School of Chemistry, University of Bristol, Bristol BS8 1TS, U.K.

Received: December 11, 1996; In Final Form: February 26, 1997[⊗]

Expressions are derived for the influence of a finite predissociation lifetime on the recoil anisotropy (β parameter) from a symmetric top parent molecule. It is found that quantum interference between transitions is important. Application of these results explains an apparent anomaly in recent measurements of the state-to-state anisotropy for NH_3 photodissociation. The theory in the limit of a long lifetime is then extended to molecules of low symmetry, showing that in favorable cases it is possible to obtain projections of the anisotropy onto more than one body-fixed axis. This has been applied to new measurements on the photodissociation process HFCO ($\tilde{A}^1A''$) → H(^2S) + FCO ($\tilde{X}^2A'$), which has been studied for excitation through rotationally structured bands in the region of 250 nm. The use of selected rotational transitions in this asymmetric top has resulted in the determination of the second moments of the recoil anisotropy of the H atoms with respect to all three inertial axes (a, b, and c). This information provides strong evidence that the predissociation is mediated by intersystem crossing to the lowest triplet state (T_1).

I. Introduction

A major object of current chemical physics research is to obtain a detailed understanding of the factors that control chemical reaction dynamics and to learn how to manipulate reactions to have a predetermined outcome. In this regard photodissociation has been considered as a *half-collision*, in that a molecule that has absorbed light breaks eventually into fragments that recoil on a repulsive potential energy surface. The ideal photochemical experiment, providing the most detailed insight into the reaction dynamics, would completely characterize at a quantum-state-resolved level both the parent molecule and the distribution of motion of the fragments.

Excitation with a polarized light source prepares an anisotropic distribution of parent molecules, facilitating the measurement of the correlation between *vector* quantities and thereby leading to stereospecific information about the fragmentation process. Where the fragments are molecular there can be mutual correlations between the excitation transition dipole (or multipole), the recoil between the fragments, and their rotational alignment.[1] For the cases that are considered in this paper one fragment is atomic so that recoil is its only vector property. Dipole excitation with linearly polarized light of an isotropic sample of molecules, even when these are all in a single rotational state, leads to the well-known distribution function

$$P(\omega_R) = [1 + \beta P_2(\cos\theta_R)]/4\pi \qquad (1)$$

where θ_R is the angle between the recoil vector **R** and the electric vector ϵ of the radiation. Most measurements of this type have involved excitation within a continuum or quasi-continuum so that the molecule dissociates rapidly on the time scale of molecular rotation. For these cases the anisotropy parameter is given by the simple relation

$$\beta = 2\langle P_2(\hat{\mathbf{R}}\cdot\hat{\mu})\rangle \qquad (2)$$

where μ is the transition dipole and P_2 a Legendre polynomial.[2] The photodissociation of H_2O,[3] HONO,[4] and H_2O_2[5,6] through excitation to their $\tilde{A}$ states all provided early examples of the use of this equation for polyatomic parent molecules.

Dissociation via predissociated states involves tunneling through a barrier or coupling to at least one more potential energy surface. If the initially excited state has a lifetime long compared with rotation, this offers the possibility of populating a single quasi-bound rotational state. The anisotropy of the ensemble of transiently excited states is then dependent not only on the direction of μ in a body-fixed frame but also on the rotational branch for excitation and the temporal nature of the exciting light. These factors are well understood for long-lived symmetric top molecules.[7] The situation is more complex when the lifetime is comparable to the rotational period (or when the molecule is an asymmetric top). Yang and Bersohn,[8] and later Nagata et al.,[9] considered the influence of a finite lifetime in terms of time-averaged correlation functions. Both these treatments dealt with the functional dependence of the anisotropy on $\omega\tau$, where ω is a rotational period and τ is the lifetime of the predissociation, but did not fully include quantum interference effects. Although these effects tend to average out for thermal molecular samples, they must be taken into account for excitation from a single quantum state.

This paper is concerned with two aspects of the recoil anisotropy for fragments from predissociated states. The effects of quantum interference on the β parameter are derived for a symmetric top parent molecule and are shown to reconcile measurements and calculations for the process $NH_3 \rightarrow NH_2 + H$ initiated through different rovibronic transitions of the NH_3 $\tilde{A}$ state. The anisotropy of a long-lived excited state of an asymmetric top is then discussed. It is shown that in principle it is possible to make separate determinations of the projection of the recoil anisotropy onto all three principal inertial axes. This theory is applied to the process HFCO($\tilde{A}^1A''$) → H + FCO. The results are used to postulate that predissociation of this excited singlet state proceeds through coupling to the continuum of the as yet unobserved $\tilde{a}^3A''$ state.

II. Theory

A. Symmetric Top with a Finite Lifetime. Choi and Bernstein have developed expressions for the spatial probability

[⊗] Abstract published in *Advance ACS Abstracts,* September 15, 1997.

S1089-5639(96)04045-5 CCC: $14.00

density function for a symmetric top molecule, and showed that if this was selected in a single long-lived $|JKM\rangle$ state it could have moments $P_n(\cos\theta)$ up to $n = 2J$.[10] This was realized experimentally for a beam of ground state CH_3I molecules, the anisotropic distribution of which was probed through ultraviolet dissociation. In this system the dissociation is prompt and highly stereospecific in the body-fixed frame, and the measurements were used to characterize the properties of the beam.[11] We wish to consider here the more complex situation when a molecule in a single quantum state is excited with monochromatic radiation within a vibronic band that has a decay lifetime comparable to the rotational period and where the coherence time of the light source is long compared with this decay time. In general the excitation will then no longer be to a pure quantum state. We will use the concept of the "Raman wave function"[12] to define the coherent superposition of rotational states for excitation from the quantum state $|\psi_i\rangle$:

$$\psi_R = \sum_j \frac{\hbar\langle j|\hat{\mu}_{ev}|i\rangle}{(\Gamma_j/2 + i\Delta_j)}\psi_j \tag{3}$$

where Γ_j is the decay constant for the jth excited state dipole-coupled to $|\psi_i\rangle$ with a frequency offset $\Delta_j = (E_j - E_i - h\nu)$. Then, following the theoretical approach of Choi and Bernstein, the probability distribution function for the symmetric top axis in space is given for any frequency by integrating over the Euler angles χ and ϕ:

$$P(\theta) = \int\int \psi_R^*\psi_R \, d\chi \, d\phi \tag{4}$$

and the absorption cross section is proportional to the complete integral.

B. Parallel Transitions. Let us first consider the case of a parallel transition, with the selection rules $\Delta M = \Delta K = 0$ and $\Delta J = 0, \pm 1$, from the initial state $|JMK\rangle$. The transition moment matrix element is given by the standard expression[2]

$$\langle J'MK|\hat{\mu}_{ev}|JMK\rangle =$$

$$(-1)^{M-K}[(2J'+1)(2J+1)]^{1/2}\begin{pmatrix} J' & 1 & J \\ M & 0 & -M \end{pmatrix}\begin{pmatrix} J' & 1 & J \\ K & 0 & -K \end{pmatrix} \tag{5}$$

Insertion of (5) into (3) then gives

$$\psi_R^*\psi_R = \hbar^2\sum_j\sum_k \frac{(2J+1)[(2J_j+1)(2J_k+1)]^{1/2}}{(\Gamma_j/2 - i\Delta_j)(\Gamma_k/2 + i\Delta_k)} \times \begin{pmatrix} J_j & 1 & J \\ M & 0 & -M \end{pmatrix}\begin{pmatrix} J_k & 1 & J \\ M & 0 & -M \end{pmatrix}\begin{pmatrix} J_j & 1 & J \\ K & 0 & -K \end{pmatrix} \times \begin{pmatrix} J_k & 1 & J \\ K & 0 & -K \end{pmatrix}\psi_{J_jKM}^*\psi_{J_kKM} \tag{6}$$

Contraction of the wave function product leads to

$$\psi_{J_jKM}^*\psi_{J_kKM} = \frac{(-1)^{M-K}}{8\pi^2}[(2J_j+1)(2J_k+1)]^{1/2}\sum_n (2n+1) \times \begin{pmatrix} J_j & J_k & n \\ M & -M & 0 \end{pmatrix}\begin{pmatrix} J_j & J_k & n \\ K & -K & 0 \end{pmatrix}D_{00}^n(\Omega)^* \tag{7}$$

Substitution of (7) into (6), integration over χ and ϕ, and noting that the imaginary contribution to (6) vanishes with summation over all values of j and k then give the result

$$\int\int \psi_R^*\psi_R \, d\chi \, d\phi = \frac{\hbar^2}{2}\sum_j\sum_k\sum_n \times \frac{(-1)^{M-K}(2J_j+1)(2J_k+1)(2J+1)(2n+1)(\Gamma_j\Gamma_k/4 + \Delta_j\Delta_k)}{(\Gamma_j^2/4 + \Delta_j^2)(\Gamma_k^2/4 + \Delta_k^2)} \times \begin{pmatrix} J_j & J_k & n \\ M & -M & 0 \end{pmatrix}\begin{pmatrix} J_j & 1 & J \\ M & 0 & -M \end{pmatrix}\begin{pmatrix} J_k & 1 & J \\ M & 0 & -M \end{pmatrix}\begin{pmatrix} J_j & J_k & n \\ K & -K & 0 \end{pmatrix} \times \begin{pmatrix} J_j & 1 & J \\ K & 0 & -K \end{pmatrix}\begin{pmatrix} J_k & 1 & J \\ K & 0 & -K \end{pmatrix}P_n(\cos\phi) \tag{8}$$

The moments of this distribution are clearly functions of both the excitation frequency and the decay constants. The absorption cross section at any frequency is given by integration over θ, to which $n = 0$ gives the only nonzero contribution.

For the common situation of an isotropic sample the various M states will be equally populated. Summation over the M-dependent factors in (8) then leads to

$$\sum_M (-1)^M\begin{pmatrix} J_j & J_k & n \\ M & -M & 0 \end{pmatrix}\begin{pmatrix} J_j & 1 & J \\ M & 0 & -M \end{pmatrix}\begin{pmatrix} J_k & 1 & J \\ M & 0 & -M \end{pmatrix} = (-1)^{n+J+K}\begin{pmatrix} 1 & 1 & n \\ 0 & 0 & 0 \end{pmatrix}\begin{Bmatrix} 1 & 1 & n \\ J_j & J_k & J \end{Bmatrix} \tag{9}$$

which is nonzero only for $n = 0$ and $n = 2$. Thus, for such an isotropic initial state the anisotropy of the transient excited state takes a form analogous to eq 1:

$$P(\Omega) = [1 + A_0P_2(\cos\theta)]/4\pi \tag{10}$$

where the spatial alignment parameter A_0 is given by:

$$A_0 = \sqrt{30}(-1)^{J+K} \times \sum_j\sum_k \left[\frac{(2J_j+1)(2J_k+1)(\Gamma_j\Gamma_k/4 + \Delta_j\Delta_k)}{(\Gamma_j^2/4 + \Delta_j^2)(\Gamma_k^2/4 + \Delta_k^2)} \times \frac{\begin{pmatrix} J_j & J_k & 2 \\ K & -K & 0 \end{pmatrix}\begin{pmatrix} J_j & 1 & J \\ K & 0 & -K \end{pmatrix}\begin{pmatrix} J_k & 1 & J \\ K & 0 & -K \end{pmatrix}\begin{Bmatrix} 1 & 1 & 2 \\ J_j & J_k & J \end{Bmatrix}}{\sum_j\left[\frac{(2J_j+1)}{(\Gamma_j^2/4 + \Delta_j^2)}\begin{pmatrix} J_j & 1 & J \\ K & 0 & -K \end{pmatrix}^2\right]}\right] \tag{11}$$

If the excitation frequency lies between the P and R lines, the various Δ_j offsets will not all have the same sign but will be the same sign outside this range. The sense of the quantum interference between the allowed transitions is therefore frequency dependent.

In the limits that all Γ_j are greater than all $|\Delta_j|$, or ν is far from resonance so that all Δ_j are approximately equal, the resonance terms in (11) can be removed from the sums. The sum rules of (3j) symbols and explicit evaluation then lead to the expected result, independent of J or K:

$$A_0(\Gamma \rightarrow \infty) = +2 \tag{12}$$

$J = K = 0$ is a special case in that there is only one possible transition, ${}^qR_0(0)$. A_0 is always $+2$ for this transition whatever the value of Γ.

In the opposite limit that all Γ_j are much smaller than the line separations, and the excitation is close to one transition,

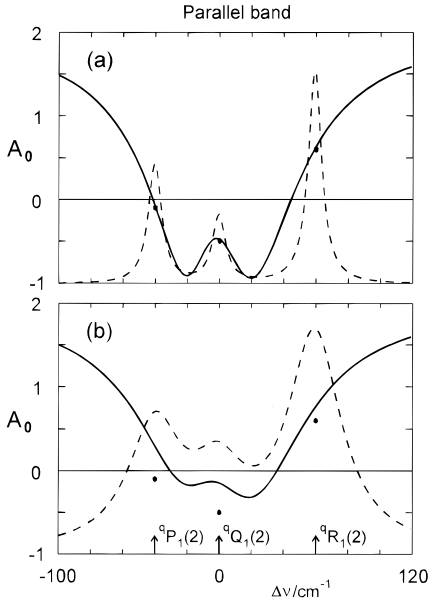

Figure 1. Frequency dependence of the spatial alignment parameter A_0 across the lifetime-broadened transitions from the $J'' = 2$, $K'' = 1$ level in a parallel band of a symmetric top: (−) A_0; (●) resonant values of A_0 for infinite lifetime; (---) excitation cross section (arbitrary scale); (a) $\Gamma = 10$ cm^{-1} for all upper levels; (b) $\Gamma = 40$ cm^{-1} for all upper levels. The rotational constant B = 10 cm^{-1}, and the origin of the frequency scale is set at the Q transition.

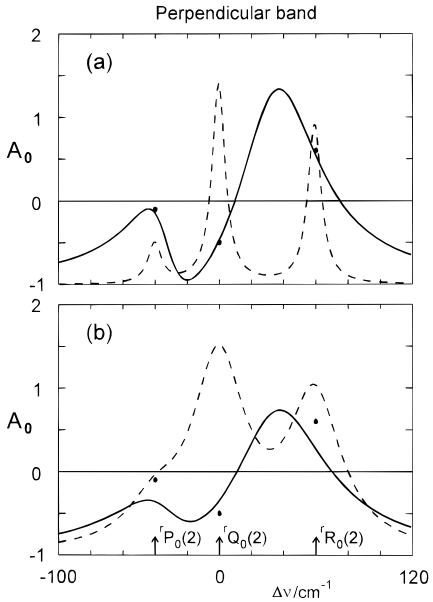

Figure 2. Frequency dependence of the spatial alignment parameter A_0 across the lifetime-broadened transitions from the $J'' = 2$, $K'' = 0$ level in a perpendicular band of a symmetric top. The upper levels are the same as in Figure 1, and all other parameters are as in Figure 1.

then only one J_j will be of importance and the interference will be negligible. The numerator and denominator in (11) then both reduce to one term with much cancellation, and A_0 takes the well-known form[7]

$$A_0(J', K \leftarrow J'', K) = t(J',J'')\left(\frac{3K^2 - J'(J'+1)}{J'(J'+1)}\right) \quad (13)$$

where the branch dependent multipliers are

$$\text{P branch} \quad t(J',J'') = -\left(\frac{J'}{2J'+3}\right) \quad (14a)$$

$$\text{Q branch} \quad t(J',J'') = +1 \quad (14b)$$

$$\text{R branch} \quad t(J',J'') = -\left(\frac{J'+1}{2J'-1}\right) \quad (14c)$$

The intermediate case is illustrated in Figure 1 for two values of the ratio of Γ to the rotational constant B and with $J'' = 2$, $K'' = 1$. It can be seen that A_0 is strongly frequency dependent over the range of finite absorption cross section even with quite sharp lines and departs significantly from the values of eq 14 with increasing Γ as the P, Q, and R lines begin to overlap, becoming generally more positive. This strong frequency dependence, even across a line, arises from the underlying tails of nonresonant transitions.

C. Perpendicular Transitions. For a perpendicular band at least one of the vibronic states must be doubly degenerate, and its rotational levels may therefore be subject to k-type doubling. Since we are principally concerned, however, with lifetime-broadened transitions, we will assume that this doubling is unresolved. The two components of the transition moment can therefore be considered independently, with matrix elements

$$\langle J'MK \pm 1|\hat{\mu}_{ev}|JMK\rangle = (-1)^{M-K-1}[(2J'+1)(2J+1)]^{1/2} \times \begin{pmatrix} J' & 1 & J \\ M & 0 & -M \end{pmatrix}\begin{pmatrix} J' & 1 & J \\ K \pm 1 & \mp 1 & -K \end{pmatrix} \quad (15)$$

Then following the development of eqs 6−11, and including the contributions from both components, the corresponding expression for the spatial alignment parameter for an isotropic sample and a perpendicular transition is

$$A_0 = \sqrt{30}(-1)^{J+K+1} \times \sum_{q=\pm 1}\sum_j\sum_k \left[\frac{(2J_j+1)(2J_k+1)(\Gamma_j\Gamma_k/4 + \Delta_j\Delta_k)}{(\Gamma_j^2/4 + \Delta_j^2)(\Gamma_k^2/4 + \Delta_k^2)} \times \begin{pmatrix} J_j & J_k & 2 \\ K+q & -K-q & 0 \end{pmatrix} \times \frac{\begin{pmatrix} J_j & 1 & J \\ K+q & -q & -K \end{pmatrix}\begin{pmatrix} J_k & 1 & J \\ K+q & -q & -K \end{pmatrix}\begin{Bmatrix} 1 & 1 & 2 \\ J_j & J_k & J \end{Bmatrix}}{\sum_{q=\pm 1}\sum_j \left[\frac{(2J_j+1)}{(\Gamma_j^2/4 + \Delta_j^2)}\begin{pmatrix} J_j & 1 & J \\ K+q & -q & -K \end{pmatrix}^2\right]} \quad (16)$$

At the limit of a very long lifetime the expressions for A_0 become identical with those for a parallel band in terms of the excited state quantum numbers J' and K'

$$A_0(J', K' \leftarrow J'', K'') = t(J', J'')\left(\frac{3K'^2 - J'(J'+1)}{J'(J'+1)}\right) \quad (17)$$

with the branch-dependent multipliers $t(J',J'')$ as in eq 14. In contrast, the limiting anisotropy for a very short lifetime (or for excitation from $J = K = 0$) is now

$$A_0(\Gamma \rightarrow \infty) = -1 \quad (18)$$

in accordance with the 90° change in the direction of the transition moment. This change in behavior reflects differences in the pattern of interferences between the parallel and perpendicular bands. This is illustrated in Figure 2, which is for r-type perpendicular excitation to the same upper states as for the parallel transitions in Figure 1. It should be noted that there is

no interference between transitions in the p-type and the r-type sub-bands, which were assumed to be well separated in generating Figure 2.

Thus, we conclude that for excitation to long-lived rovibronic states the spatial alignment depends on ΔJ and the upper state quantum numbers but not on the vibronic nature of the transition and its associated ΔK, whereas for more short-lived states these latter factors have an important and frequency-dependent influence on the anisotropy.

D. Long-Lived Rotational States of an Asymmetric Top. The fragmentation pattern of an asymmetric top may no longer have axial symmetry about any particular body-fixed direction. We will show that in favorable cases it is possible to derive values of the second moments of this distribution about all three inertial axes. This is only possible for excitation through spectra that have well-resolved rotational structure. We note from above that on resonance in such a situation we need to consider only ΔJ and the resonant wave functions of the excited state, since quantum interference between transitions is then negligible. Such a rotational wave function can be expressed in a principal axis system as

$$\psi'_M = \sum_{K=-J}^{J} c_K |JKM\rangle \tag{19}$$

where the values of the c_K coefficients will depend on the choice of body-fixed z axis but will be nonzero for any one level either for only even values of K or for only odd values of K, depending on its parity.

The probability distribution function for such a single M state will be

$$P_M(\Omega) = \psi'_{\mathrm{M}}{}^*\psi'_{\mathrm{M}} = \frac{(2J+1)}{8\pi^2}\sum_n (2n+1)\begin{pmatrix} J & J & \mathrm{n} \\ \mathrm{M} & -M & 0 \end{pmatrix} \times \sum_m \sum_j \sum_k (-1)^{M-K_k} c_j^* c_k \begin{pmatrix} J & J & \mathrm{n} \\ \mathrm{K_j} & -K_k & m \end{pmatrix} C_{nm}(\theta\chi) \tag{20}$$

where $C_{nm}(\theta\chi)$ is a spherical harmonic. Note that this function is independent of ϕ, the angle about the electric field vector, as it should be, but does vary with the body-fixed angle χ. We have seen above that for a long-lived rotational state the K dependence of the transition moment matrix element defines the intensity of a transition and the M dependence its spatial anisotropy (see eqs 5 and 15). For an isotropic sample in the lower state we may again multiply eq 20 by these M-dependent terms and make the summation over M of eq 9. This limits n to 0 and 2 as before, and the all-even or all-odd character of K limits m to 0 or ± 2. Integration over ϕ, and normalization, then leads to

$$P(\theta\chi) = \frac{1}{4\pi}\left[1 + (-1)^{J''}\sqrt{30}(2J+1)\begin{Bmatrix} 1 & 1 & 2 \\ J & J & J'' \end{Bmatrix} \times \sum_{m=0,\pm 2} \sum_j \sum_k (-1)^{K_k} c_j^* c_k \begin{pmatrix} J & J & 2 \\ K_j & -K_k & m \end{pmatrix} C_{2m}(\theta\chi)\right] \tag{21}$$

Thus the rotational anisotropy can no longer be characterized solely in terms of A_0, and the generalization of eq 10 is

$$P(\theta\chi) = [1 + A_0 C_{20}(\theta\chi) + A_2\{C_{22}(\theta\chi) + C_{2-2}(\theta\chi)\}]/4\pi \tag{22}$$

It will prove convenient to relate A_0 and A_2 to body-fixed expectation values of angular momentum operators, which are generated by most asymmetric top programs. For the wave function of eq 19

$$\langle\psi'|3\hat{J}_z^2 - \hat{J}^2|\psi'\rangle = \sum_j (-1)^{J-K_j}[(2J-1) \times J(2J+1)(J+1)(2J+3)]^{1/2} c_j^* c_j \begin{pmatrix} \mathrm{J} & \mathrm{J} & 2 \\ K_j & -K_j & 0 \end{pmatrix} \tag{23a}$$

and

$$\langle\psi'|\hat{J}_x^2 - \hat{J}_y^2|\psi'\rangle = \sum_{m=\pm 2}\sum_j\sum_k (-1)^{J-K_k} \times \left[\frac{(2J-1)J(2J+1)(J+1)(2J+3)}{6}\right]^{1/2} c_j^* c_k \begin{pmatrix} J & \mathrm{J} & 2 \\ K_j & -K_k & m \end{pmatrix} \tag{23b}$$

Comparison of eqs 21−23, and expansion of the $\{6j\}$ symbol give the desired equations

$$A_0 = t(J',J'')\frac{\langle\psi'|3\hat{J}_z^2 - \hat{J}^2|\psi'\rangle}{J'(J'+1)} \tag{24a}$$

and

$$A_2 = t(J',J'')\sqrt{\frac{3}{2}}\frac{\langle\psi'|\hat{J}_x^2 - \hat{J}_y^2|\psi'\rangle}{J'(J'+1)} \tag{24b}$$

Near-prolate or near-oblate tops exhibit a first-order asymmetry splitting only for $K = 1$, where K is referred to the a- or c-axis, respectively. A_2 will therefore be significant only for transitions to such levels.

E. Anisotropy of the Fragmentation. A full quantum mechanical approach to photodissociation would treat the excitation and dissociation as a single coherent process.[13] However, we are concerned here with situations in which there is a clear separation in time scales between rotation in a quasi-bound state and rapid fragmentation following predissociation. The body-fixed fragmentation distribution can then be mapped onto the β parameter of eq 1 through the spatial anisotropy of excitation to the long-lived excited rotational state of the parent molecule. Let this normalized angular distribution for fragmentation be expanded over spherical harmonics in the body-fixed frame:

$$P(\beta\alpha) = \sum_{k,q}\frac{(2k+1)}{4\pi}a_{kq}C_{kq}(\beta\alpha) \tag{25}$$

where

$$a_{00} = 1 \quad \text{and } a_{kq} = \langle C_{kq}(\beta\alpha)^*\rangle \tag{26}$$

with β and α as the polar angles of the recoil vector **R** in this frame. Each term in (25) must be rotated to the space-fixed frame

$$C_{kq}(\beta\alpha) = \sum_\lambda C_{k\lambda}(\omega_{\mathrm{R}})D^k_{\lambda q}(\Omega) \tag{27}$$

before insertion into the integral for the space-fixed distribution:

$$P(\omega_{\mathrm{R}}) = \int P(\Omega)P(\beta\alpha)\,\mathrm{d}\Omega \tag{28}$$

Use of the angular momentum addition theorem then results in

$$P(\omega_R) = [1 + \{A_0 a_{20} + A_2 a_{22}^+\} P_2(\cos\theta_R)] \quad (29)$$

with

$$a_{22}^+ = a_{22} + a_{2-2} \quad (30)$$

Thus for a long-lived predissociated rotational state of an asymmetric top the generalization of eq 2 is

$$\beta = A_0 a_{20} + A_2 a_{22}^+ \quad (31)$$

where the two expectation values that can be determined in this case are

$$a_{20} = \left\langle \frac{1}{2}(3\cos^2\beta - 1) \right\rangle \quad \text{and} \quad a_{22}^+ = \left\langle \sqrt{\frac{3}{2}} \sin^2\beta \cos 2\alpha \right\rangle \quad (32)$$

Butenhoff *et al.* have derived an equation analogous to eq 31, and applied this to the anisotropy of recoil of H_2 generated by predissociation of rovibronic levels of the S_1 state of H_2CO.[14] These authors did not, however, make the direct connection between the A_0 and A_2 parameters and the body-fixed expectation values of the angular momentum operators (eqs 24a and 24b).

It is not essential for the body-fixed anisotropy to be referred to the choice of axis frame that is most convenient for describing the energy levels of an asymmetric top, provided that A_0, A_2, and the a_{nm} parameters are referred to the same frame. Indeed in the analysis below we find it convenient to refer measurements from different transitions to expectation values in a Cartesian representation:

$$a_{2a} = \left\langle \frac{1}{2}(3\cos^2\beta - 1) \right\rangle \equiv a_{20} \quad (33a)$$

$$a_{2b} = \left\langle \frac{1}{2}(3\sin^2\beta\cos^2\alpha - 1) \right\rangle \equiv \left(-\frac{1}{2}a_{20} + \sqrt{\frac{3}{8}}a_{22}^+ \right) \quad (33b)$$

$$a_{2c} = \left\langle \frac{1}{2}(3\sin^2\beta\sin^2\alpha - 1) \right\rangle \equiv \left(-\frac{1}{2}a_{20} - \sqrt{\frac{3}{8}}a_{22}^+ \right) \quad (33c)$$

with the constraint that

$$a_{2a} + a_{2b} + a_{2c} = 0 \quad (34)$$

III. Quantum Interference in the Photodissociation of Ammonia

The photodissociation of ammonia following excitation through the $\tilde{A}-\tilde{X}$ band system has received much attention.[15] This provides one of the best examples of vector correlations fully resolved at a quantum state level in both the parent and the fragment. Figure 3 gives a representative example of a total kinetic energy release (TKER) spectrum for the H−NH_2 products resulting from fragmentation of a jet-cooled sample of NH_3 molecules for two angles θ_R between the electric field vector ϵ and the time-of-flight (TOF) axis **R**. The anisotropy parameter β is a strongly variable function of the internal energy state of the NH_2 fragment. Data such as these have been interpreted in terms of an impact parameter model.[15] This treats NH_3 as a pseudotriatomic molecule [$(H_2)-N-H$] and assumes that all product angular momentum is established at a point of conical intersection between the $\tilde{X}$ and $\tilde{A}$ potential energy surfaces of the dissociating parent molecule. This model accounted well for the variation of β with the internal energy

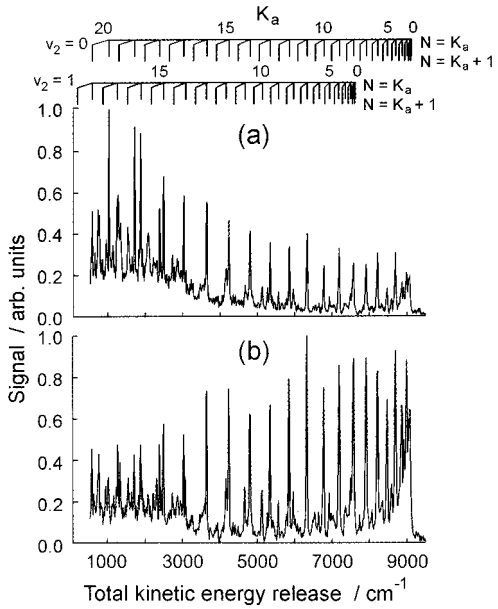

Figure 3. TKER spectra for the H−NH_2 products resulting from fragmentation of a jet-cooled sample of NH_3 molecules following photolysis through the overlapping $^qR_0(1)$ and $^qR_1(1)$ transitions at 46 200 cm^{-1} in the 0_0^0 band of the $\tilde{A}^1A_2-\tilde{X}^1A_1$ band system: (a) $\theta_R = 0°$; (b) $\theta_R = 90°$.

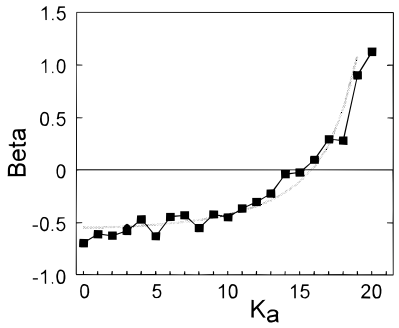

Figure 4. Variation of the recoil anisotropy parameter β with NH_2 angular momentum, for the channels leading to H + $NH_2(\tilde{X},\nu_2,N = K_a)$ products, resulting from photolysis of NH_3 at 46 200 cm^{-1} as illustrated in Figure 3. The smooth curve shows the result of calculations using an impact parameter model with an empirically chosen mean value of $A_0 = +1.1$.

of NH_2. Even so, there was some inconsistency in values derived from different rovibronic states of the parent NH_3.

Excitation from $J'' = 0$ within this parallel band system has the advantage that $A_0 = 2$ independent of the excited state lifetime (section II. B above). Unfortunately, there is no transition from $J'' = 0$ in the origin band because of the restrictions of nuclear statistics, but there is such a $^qR_0(0)$ transition within the 2^1_0 band. This latter transition is free from overlapping, and the measured values of β for channels leading to H + $NH_2(v_2 = 0, N = K_a)$ cover almost the complete range from −1 to +2. The impact parameter model predicts that the H atom is ejected in the NH_3 plane if its partner NH_2 molecule is in a low angular momentum state but perpendicular to this plane for a high angular momentum state. The corresponding values of a_{20} range from close to −0.5 for high TKER (low K_a state of NH_2) to almost +1.0 for the lowest TKER (high K_a). The combination of these values of a_{20} with $A_0 = 2$ gives a good overall fit to the data. A time-dependent quantum mechanical study of this same system also reproduces these same trends, lending further credence to this model.[16]

Anisotropy measurements have also been made using excitation to the lowest available J states within the origin band

through the overlapping $^qR_0(1)$ and $^qR_1(1)$ transitions (computed separation of 1.2 cm^{-1}).[15] The first of these has about twice the transition intensity of the second, and the long lifetime values of A_0 are +1.0 and +0.5, respectively, with a weighted mean of 0.83. However, the model gives a good fit to the data using an empirical value of $A_0 = +1.1$, a difference of over 30% (Figure 4). Now the measured value of Γ for these transitions is 34 cm^{-1}, and the excited state B value is 9.7 cm^{-1}. When quantum interference is allowed for using eq 11, these values of A_0 are changed to +1.113 and +0.916, respectively, with a weighted mean of +1.05. Thus, bearing in mind the rapid variation in A_0 across a broadened transition (Figure 1) and the possibility that the laser frequency may not have been at the center of the overlapping lines, the apparent inconsistency between measurements within the 0^0_0 and 2^1_0 bands[15] stemmed from the neglect of quantum interference, and not from a change in the body-fixed trajectories.

IV. Photodissociation of HFCO ($\tilde{A}^1A''$) to H + FCO

Formyl fluoride, HFCO, has a highly structured ultraviolet band system, stretching from an origin at 267 nm to at least 200 nm, arising from the carbonyl (π^*-n) electronic promotion. Vibrational and rotational analyses show that the molecule is planar in the ground state but pyramidal in the excited state. The barrier to inversion in the excited state is sufficiently low that the transition is best classified in the C_s point group as $\tilde{A}^1A''-\tilde{X}^1A'$.

When excited within this band system, formyl fluoride may undergo a number of unimolecular processes:

$$\mathrm{HFCO}(\tilde{X}^1A') \xrightarrow{h\nu_1}$$

$$\mathrm{HFCO}(\tilde{A}^1A'') \rightarrow \mathrm{HFCO}(\tilde{X}^1A') + h\nu_2 \quad \text{(LIF)} \quad (35a)$$

$$\rightarrow \mathrm{HF}(X^1\Sigma^+) + \mathrm{CO}(X^1\Sigma^+) \quad (35b)$$

$$\rightarrow \mathrm{H}(^2S) + \mathrm{FCO}(^2A') \quad (35c)$$

$$\rightarrow \mathrm{F}(^2P) + \mathrm{HCO}(^2A') \quad (35d)$$

$$\rightarrow \mathrm{HFCO}(\tilde{X}^1A') \quad \text{(IC)} \quad (35e)$$

$$\rightarrow \mathrm{HFCO}(\tilde{a}^3A'') \quad \text{(ISC)} \quad (35f)$$

The most extensive study of the photochemistry of HFCO has used stimulated emission pumping from the $\tilde{A}$ state to populate high rovibrational levels of the ground state in competition with the above processes.[17−19] These levels lie below the thresholds for the radical channels eqs 35c and 35d and result exclusively in fragmentation to the molecular channel (eq 35b). This is also the major channel for thermal dissociation with an activation energy of *ca.* 180 kJ/mol.[20,21] An early study with broad-band UV irradiation produced HF with an inverted vibrational population, but the other dissociation channels were not investigated.[22] More recently, excitation at 248 and 193 nm gave the radical channels as the major products.[23] There was also some evidence that H + F + CO may be produced after 193 nm excitation. Thus, these excited state dissociations show completely different features from the ground state (thermal) reactions.

The thermodynamic threshold for process 35c is at 286 nm (see below). The heat of formation of FCO is not known with good precision, but the threshold for process 35d will be at a shorter wavelength. The H + FCO channel is therefore the only radical channel open for the lower vibronic levels of the $\tilde{A}-\tilde{X}$ band system. We have embarked on an extensive study of this channel and its competition with LIF (eq 35a).[25]

A. Experimental Section. Formyl fluoride was generated by the reaction between cyanuric fluoride and formic acid[24] and stored at liquid nitrogen temperature when not in use. A cold beam of HFCO was produced by flowing helium at a pressure of *ca.* 2 atm over the liquid at dry ice temperature and expanding this into a molecular beam apparatus through a pulsed nozzle (General Valve Co.). Laser-induced fluorescence was excited with a frequency-doubled pulsed dye laser (Spectra Physics PDL3 operating on a variety of dyes, with a BBO crystal in a home-built autotracker) and detected in a right angled geometry. H atoms were detected by 2 + 1 REMPI excited at 243 nm, using a frequency-doubled dye laser (Spectron SL803 operating with DCM dye) followed by mixing in BBO with residual 1064 nm radiation from the Nd:YAG pump laser, and counter-propagated against the excitation laser. The source region of the ions was surrounded by a constant field box of grid wires, and the ions were accelerated along a TOF path of length 315 mm. The H^+ ion signal was well removed from that of heavier ions.

For recording H atom yield spectra the mass spectrometer was operated in a high-field Wiley−McLaren configuration.[26] We also attempted to use this configuration for measuring the Doppler profiles of the H atom line following photolysis through various HFCO transitions but with limited success. It was found that the H atoms are ejected with a velocity of *ca.* 11 km/s. Consequently, at the wings of the H atom lines the ion trajectories could move off the TOF axis by more than 1 cm during the flight time, and those detected were drawn from widely different portions of the molecular beam as the Doppler profile was scanned, thereby distorting the profiles. This was avoided by setting the 243 nm laser at line center, using a low extraction field (typically 0.8 V/mm or 1.2 V/mm), and partially resolving the recoil velocity structure of the TOF profiles. For these low-field measurements a slit 20 mm × 2 mm, with its long axis parallel to the molecular beam and perpendicular to the laser beams and situated 105 mm from the ion source in the field-free section of the flight path, served to define the accepted trajectories. All ions that passed through this slit were detected by a Johnston multiplier of 25 mm diameter, with signal processing by a digital oscilloscope having a 10 ns time resolution (LeCroy 9310A). The polarization of the dissociation laser could be set parallel or perpendicular to the TOF axis using a photoelastic modulator (Hinds Inc. PEM80). This had the advantage that beam overlaps were undisturbed by the switch in polarization so that reliable estimates of β values could be extracted from pairs of line profiles.

A complementary series of experiments is in process in our laboratory in which high-resolution H atom TOF spectra are being recorded at a number of excitation wavelengths.[27] These data confirm our own information on the energy disposal and give a much more accurate value for the dissociation energy to H + FCO, but unfortunately, the resolution of the dissociation laser was insufficient to yield meaningful data on the anisotropy of the dissociation.

B. Excitation Spectra. The laser-induced fluorescence spectra recorded at wavelengths longer than 253 nm were very similar to those recently described by Choi[28] and by Crane *et al.*[29] They were accurately simulated as asymmetric top bands with a sample temperature of 3 K. Most of the strong bands are of type *c*, involving symmetric ν_6^+ excitation of the out-of-plane inversion vibration in the excited state, with weaker type *a* or type *b* bands involving ν_6^- excitation. H atoms could not be detected in this spectral region but show a sharp onset

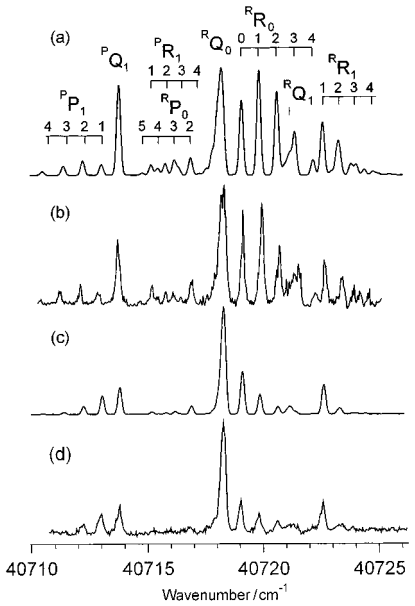

Figure 5. Experimental and simulated excitation spectra for the $2_0^1 5_0^1 6_0^{2+}$ band in the $\tilde{A}^1A''-\tilde{X}^1A'$ system of HFCO: (a) simulated H atom action spectrum; (b) experimental H atom action spectrum; (c) simulated LIF spectrum; (d) experimental LIF spectrum. The simulations are based on the assumption that the rate of dissociation to H + FCO increases linearly with the expectation values for $\langle J_b^2 \rangle$ in the excited states with a thermal sample at 3 K.

at about 39 690 cm^{-1}. Detailed band simulations place this threshold at between 39 689.3 and 39 691.8 cm^{-1} above the lowest level of the ground state. Above this frequency most of the LIF spectra, and many of the H atom REMPI action spectra, depart significantly in band profile from simulations using thermal equilibrium, but in complementary ways. Close to the H atom appearance threshold the effects tend to be random within the rotational structure of a band, suggesting resonances with an underlying "lumpy continuum" of dark levels. A few hundreds of cm^{-1} higher these effects become more systematic and can be simulated by assuming that the rate of dissociation, in competition with fluorescence, increases with J_b^2 (Figure 5). Crane *et al.* have found that the excited state lifetimes measured by LIF decrease with increasing energy presumably because of increasing competition by the nonradiative pathways.[29] We have found that the intensity of LIF emission becomes too weak to be recorded above 42 000 cm^{-1} but have recorded H atom action spectra up to 43 800 cm^{-1}.

The Doppler profiles of the H atom line, even following dissociation close to the H atom appearance threshold, indicated that about 5000 cm^{-1} is then released as recoil energy. The high-resolution H atom TOF study[27] places the dissociation energy D^0_0(H−FCO) at 34 950 cm^{-1} and also demonstrates that close to threshold the spread of internal energies of the partner FCO radical is limited to energies less than about 1000 cm^{-1}. It is this high recoil energy and low velocity spread that have made possible the measurement of the recoil anisotropy through TOF measurements.

C. H Atom TOF Profiles and the Recoil Anisotropy. Time-of-flight line profiles have been recorded for several transitions within three vibronic bands. The rotational anisotropy parameters for selected transitions within type *c* bands, computed using eq 24, are given in Table 1. These transitions were selected as having the most extreme anisotropy. In each case this anisotropy has axial symmetry about one of the principal axes of rotation. For this reason the A_0 and A_2 parameters are given in Table 1 in terms of each of the three possible representations. Thus, the three Cartesian parameters

TABLE 1: Rotational Anisotropy Parameters for Selected Transitions of a Type *c* Band

	type-I representation		type-II representation		type-III representation	
transition	A_0	A_2	A_0	A_2	A_0	A_2
$^rR_0(0)$	−1	$-(3/2)^{1/2}$	−1	$+(3/2)^{1/2}$	+2	0
$^rR_0(1)$	+1/2	$-(3/8)^{1/2}$	−1	0	+1/2	$+(3/8)^{1/2}$
$^pQ_1$(all J)	−1	0	+1/2	$+(3/8)^{1/2}$	+1/2	$-(3/8)^{1/2}$

of the body-fixed fragmentation anisotropy can be determined using

$$\beta(^rR_0(0)) = +2a_{2c} \tag{36a}$$

$$\beta(^rR_0(1)) = -a_{2b} \tag{36b}$$

$$\beta(^pQ_1(\text{all } J)) = -a_{2a} \tag{36c}$$

The two ^rR transitions are single unoverlapped lines, and although the lines of the $^pQ_1$branch are completely overlapping at the resolution of our laser, they fortunately all have the same anisotropy parameters. This use of three transitions provides a check through the sum rule of eq 34.

Several pairs of profiles were recorded for each chosen transition, each being one measurement in parallel polarization and one in perpendicular polarization made in rapid succession with no other instrumental change. The extraction field was a compromise between being low enough that the anisotropy of recoil gave a good spread of arrival times and being high enough that few ion trajectories were cut off by the finite height of the slit between the source and detection chambers. An additional experimental problem arose from imperfect laser beam quality, and the need to ensure a good overlap between the photolysis beam and the analysis beam, which was focused with a 50 cm lens. The analysis pulse was also delayed by about 20 ns with respect to the photolysis pulse to allow for the known HFCO excited state lifetimes on the order of 10 ns. In principle the TOF peaks should be symmetric about their centers, apart from a slight distortion by the detection electronics, which had been calibrated using a fast pulse generator. In practice the profiles were rarely completely symmetrical.

Each pair of profiles was therefore analyzed by simulation as follows. A three-dimensional swarm of initial trajectories were set up with the velocity distribution indicated by the high-resolution H atom TOF measurements and given a probability distribution as in eq 1 with a trial value of β for both parallel and perpendicular polarizations. These were further weighted by a Gaussian function representing the selection of the velocity component parallel to the analysis beam, the 1.2 cm^{-1} fwhm of which was much less than the Doppler width of *ca.* 3.4 cm^{-1}. The path of each trajectory through the electric fields of the mass spectrometer was computed, and its weight was added to an appropriate 10 ns time-of-arrival bin if it passed through the slit. The two complete profiles were then convoluted with the response function of the electronics. Two additional options in the fitting program were found to be advantageous in comparing the computed and experimental profiles to allow for the problems outlined above. Each profile was symmetrized with respect to the center point of its full width at half maximum, with the assumption that any distortion between initial forward and backward trajectories did not change with the switch in polarization. The sums and differences of each parallel/perpendicular pair were then computed. The ratio of the integrated experimental and simulation sum functions was then used to scale the simulated difference function for comparison

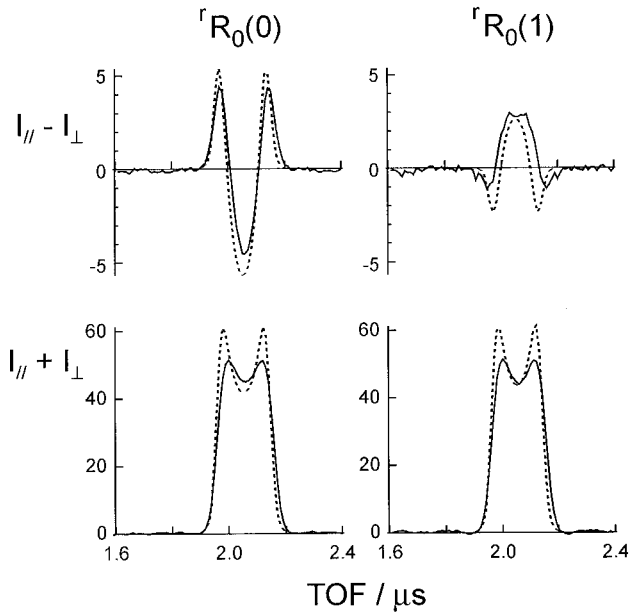

Figure 6. Sums and differences of the time-of-flight profiles of H atoms with parallel and perpendicular polarization following photolysis of HFCO via two lines in the $2_0^1 4_0^1 5_0^2$ band of the $\tilde{A}-\tilde{X}$ system: (−) experimental profile; (---) simulation. The extraction field for these records was 1.2 V/mm.

TABLE 2: Experimental Measurements of the Anisotropy Parameters for HFCO* → H + FCO

	band		
	40 279 cm^{-1} ($2_0^1 6_0^{2+}$)	40 586 cm^{-1} ($2_0^1 4_0^1 5_0^2$)	40 718 cm^{-1} ($2_0^1 5_0^1 6_0^{2+}$)
$\beta(^rR_0(0))^a$	−0.02	+0.24	+0.38
$\beta(^rR_0(1))^a$	−0.40	−0.10	+0.01
$\beta(^pQ_1(\text{all J}))^a$	+0.09	+0.26	+0.17
a_{2a}	−0.09	−0.26	−0.17
a_{2b}	+0.40	+0.10	−0.01
a_{2c}	−0.01	+0.12	+0.19
$\langle\alpha\rangle$ (type I rep.)^b	36°	45°	50°
$\langle\beta\rangle$ (type I rep.)^b	74°	64°	62°

^{a} Typical error in β values is ±0.02. ^{b} Derived from a_{2b} and a_{2c}.

with experimental results. Finally, a least-squares routine was used to determine the value of β that optimized this fit. This process was iterated until stable.

Figure 6 illustrates one such set of experimental and simulated TOF profiles, and the mean values of the measurements for each transition are summarized in Table 2. For each set of measurements the values of a_{2b} and a_{2c} are derived from isolated single spectral lines, whereas a_{2a} is derived from a Q branch of overlapping lines. We have therefore chosen to derive expectation values of $\langle\alpha\rangle$ and $\langle\beta\rangle$ in a type I representation from a_{2b} and a_{2c} using eqs 33b and 33c, and use a_{2a} as a consistency check. $\langle\alpha\rangle$ is the mean azimuthal angle of **R** measured from the (*a*,*b*) inertial plane, and $\langle\beta\rangle$ is the mean angle with respect to the *a*-axis. It should be stressed here that if fragmentation takes place over a wide range of body-fixed angles, then the values of $\langle\alpha\rangle$ and $\langle\beta\rangle$ thus derived may be displaced from the values for the most probable fragmentation.

The measurements from the two $^rR_0$ lines show a consistent trend with increase in the excitation frequency and thus a systematic trend in the mean angles. The consistency check from the $^pQ_1$ branch is very good for the 40 718 cm^{-1} band. It is less good for the 40 586 cm^{-1} band, but an alternative value of $\langle\beta\rangle$ derived from a_{2a} using eq 33a only leads to an increase of 3°. Both of these bands have an intensity distribution in both LIF and H atom detection that can be accurately simulated

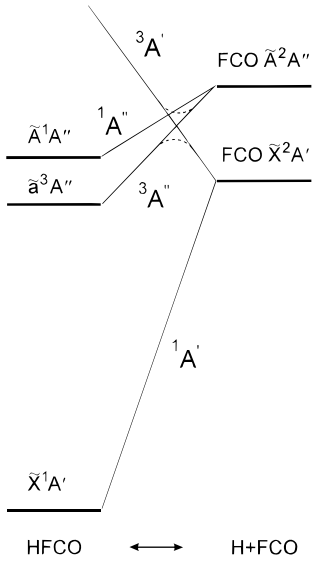

Figure 7. Schematic correlation diagram for HFCO → H + FCO: (−) planar geometry of point group C_s; (---) pyramidal geometry of point group C_1. The crossing of the $^3A''$ and $^3A'$ surfaces for planar geometries leads to a conical intersection with respect to the out-of-plane coordinate.

with global parameters. In contrast, only the sign of a_{2a} is consistent with expectation for the 40 279 cm^{-1} band. However, we note that the intensity of the $^pQ_1$ branch in this band is anomalous in comparison with its simulation and suspect a local perturbation. An alternative possibility is that close to threshold there is time for futher parent rotation after the radiationless transition to the predissociating state, as indicated by the observation of a lumpy continuum close to the threshold. With Coriolis coupling as a contributory factor to the rate of predissociation, this would imply a *J*-dependent change in the parent rotational anisotropy. Since the various a_{2q} parameters are derived from different transitions, the sum rule of eq 34 would then no longer be valid. Certainly, the best fit to the sum rule of eq 34 is for the set of data with the highest excitation energy.

D. Discussion

The aim of this study of the recoil anisotropy was to gain an understanding of the dissociation dynamics. We begin by considering the potential energy surfaces that may be involved. Figure 7 is a schematic representation of the state correlations for HFCO → H + FCO for planar and pyramidal geometries. This shows that the ground state of HFCO correlates with ground state products but that the $\tilde{A}^1A''$ state correlates with excited state products, which are too high in energy to be accessible at the energies of our experiments. The so far unobserved $\tilde{a}^3A''$ state also correlates with these same products in a planar geometry but with the ground state products in a pyramidal geometry. The two possible mechanisms whereby the $\tilde{A}^1A''$ state can dissociate are therefore internal conversion (IC) to the continuum of the $\tilde{X}^1A'$ state (process 35e) or intersystem crossing (ISC) to the $\tilde{a}^3A''$ state (process 35f). Let us consider these in turn.

Internal conversion to the ground state is possible at all energies within the $\tilde{A}^1A''$ state. Evidence that this does occur to some extent comes from the excited state lifetimes reported by Crane *et al.*[29] using excitation at the peak LIF intensity of each band. These show a downward trend from 130 ns for the origin band to 17 ns just below the threshold determined above for fragmentation via the radical channel. However, we know from the work of Moore et al.[17−19] that high levels of the ground

state fragment via the molecular channel 35b. Furthermore, from the correlation diagram of Figure 7 we would not predict a barrier of *ca.* 5000 cm^{-1} to dissociation on the ground state surface to give H + FCO, and there is no such barrier in the *ab initio* study referred to below.

The conical intersection on the path from the $\tilde{a}^3A''$ state to H + FCO($\tilde{X}$) will inhibit dissociation on this surface for planar geometries, and its residual influence in pyramidal geometries could account for a barrier on the minimum energy path to dissociation. Sumathi and Chandra[30] have used *ab initio* quantum chemical methods to study the decomposition on this surface. They do indeed find that there is a barrier to this dissociation with a pyramidal transition state. Their best estimates cannot be considered to be quantitatively correct, since they predict an available energy of 14 000 cm^{-1} from the transition state to the ground state products compared with our experimental value of 5000 cm^{-1}. Even so, their three different *ab initio* methods lead to very similar structures at the transition state, and the following discussion uses the parameters of the best of these (UHF-6-31 G*/MP2).

Consider the possible dissociation mechanism close to the threshold for the radical channel. All vibrational levels of the $\tilde{A}$ state are subject to a large amplitude of the out-of-plane motion, and the rotational probability distribution will relate to the mean inertial frame. After extensive rotation, let there be a prompt electronic rearrangement to the $\tilde{a}$ state followed by a rapid passage along the minimum energy path. The distribution function for the inertial frame at the transition state will therefore be the same as it was in the $\tilde{A}$ state. We calculate from the theoretical geometry that the angles of the elongated C−H vector with respect to its inertial frame are

$$\text{HFCO}(\tilde{a}) \rightarrow \text{H} + \text{FCO (transition state)}$$
$$\alpha = 37.7°, \beta = 74.4° \quad (37)$$

If dissociation occurred along this C−H vector, then **R** would make these same angles to the original inertial frame. The angles of eq 37 are remarkably close to those determined for dissociation via the vibronic level closest to the threshold (Table 2). Sumathi and Chandra do comment[30] that the reaction coordinate near the saddle point is primarily a stretching of the C−H bond but also that the H atom may swing off toward the perpendicular to the FCO plane (N.B. this is not the instantaneous *a,b* plane). An increasing tendency to such a swing could explain the observed trend in $\langle\alpha\rangle$ with increasing energy.

Thus, all the evidence points to intersystem crossing as the predissociation mechanism that opens up the radical channel at the energies of our measurements.

V. Conclusion

This paper has presented a theoretical treatment of the influence of quantum interference on the spatial anisotropy of a predissociating symmetric top molecule. This explains an apparent 30% discrepancy between state-to-state recoil anisotropy measurements of H atoms produced via different rovibronic state of $NH_3(\tilde{A}^1A'')$. This theory is then extended in the long lifetime limit to asymmetric top molecules. It is shown that it is possible in principle to determine the second moments with respect to all three inertial axes of the anisotropy of fragment recoil following predissociation. Experimental measurements of this anisotropy for $HFCO(\tilde{A}^1A'') \rightarrow H + FCO(\tilde{X})$ via predissociating levels show that the reaction proceed via intersystem crossing and dissociation on the surface of the lowest triplet state. The theoretical analysis presented in this paper should find application to the photodissociation dynamics of many other small parent molecules.

Acknowledgment. We are indebted to the NERC for financial support for this research and for a studentship to one of us (T.W.R.H.). R.N.D. thanks the Leverhulme Trust for the award of an emeritus fellowship. We are grateful to Professor C. B. Moore and his collaborators for advance communication of their results and for a short period that T.W.R.H. spent in their laboratory. Finally, we thank our Bristol colleagues K. N. Rosser and C. Reed, respectively, for technical advice and the communication of preliminary results.

References and Notes

(1) Dixon, R. N. *J. Chem. Phys.* **1986**, *85*, 1866.
(2) Zare, R. N. *Angular Momentum*; Wiley Interscience: New York, 1988.
(3) Andresen, P.; Ondrey, G. S.; Titze, B.; Rothe, E. W. *J. Chem. Phys.* **1984**, *80*, 2548.
(4) Vasudev, R.; Zare, R. N.; Dixon, R. N. *J. Chem. Phys.* **1984**, *80*, 4863.
(5) Gericke, K-H.; Klee, S.; Comes, F. J.; Dixon, R. N. *J. Chem. Phys.* **1986**, *85*, 4463.
(6) Docker, M. P.; Hodgson, A.; Simons, J. P. *Faraday Discuss. Chem. Soc.* **1985**, *82*, 25.
(7) Greene, C. H.; Zare, R. N. *Annu. Rev. Phys. Chem.* **1982**, *33*, 119.
(8) Yang, S. E.; Bersohn, R. *J. Chem. Phys.* **1974**, *61*, 4400.
(9) Nagata, T.; Kondow, T.; Loge, G. W.; Zare, R. N. *Mol. Phys.* **1983**, *50*, 49.
(10) Choi, S. E.; Bernstein, R. B. *J. Chem. Phys.* **1986**, *85*, 150.
(11) Bernstein, R. B.; Choi, S. E.; Stolte, S. *J. Chem. Soc., Faraday Trans. 2* **1989**, *85*, 1097.
(12) Krishna, R. M. V.; Coalson, R. D. *Chem. Phys.* **1988**, *120*, 327.
(13) Balint-Kurti, G. G.; Shapiro, M. *Chem. Phys.* **1981**, *61*, 137.
(14) Butenhoff, T. J.; Carleton, K. L.; van Zee, R. D.; Moore, C. B. *J. Chem. Phys.* **1991**, *94*, 1947.
(15) Mordaunt, D. H.; Ashfold, M. N. R.; Dixon, R. N. *J. Chem. Phys.* **1996**, *104*, 6460; and references therein.
(16) Dixon, R. N. *Mol. Phys.* **1996**, *88*, 949.
(17) Choi, Y. S.; Moore, C. B. *J. Chem. Phys.* **1991**, *94*, 5414.
(18) Choi, Y. S.; Moore, C. B. *J. Chem. Phys.* **1992**, *97*, 1010.
(19) Choi, Y. S.; Moore, C. B. *J. Chem. Phys.* **1991**, *103*, 9981.
(20) Samsonov, Y. N.; Petrov, A. K. *Kinet. Katal.* **1981**, *32*, 575.
(21) Saito, K.; Kuroda, H.; Nakumoto, T.; Munechika, H.; Murakami, I. *Chem. Phys. Lett.* **1985**, *113*, 399.
(22) Klimek, D. E.; Berry, M. J. *Chem. Phys. Lett.* **1973**, *20*, 141.
(23) Weiner, B. R.; Rosenfeld, R. N. *J. Chem. Phys.* **1988**, *92*, 4640.
(24) Olah, G. A.; Nojima, M.; Kerekes, I. *Synthesis* **1973**, 487.
(25) Hancock, T. W. R. Ph.D. Thesis, University of Bristol, Bristol, U.K., 1997. Hancock, T. W. R.; Dixon, R. N. *J. Chem. Soc., Faraday Trans.* **1997**, *93*, 2707.
(26) Wiley, W. C.; McLaren, I. M. *Rev. Sci. Instrum.* **1955**, *26*, 1150.
(27) Reed, C.; Kono, M.; Langford, S.; Hancock, T. W. R.; Dixon, R. N.; Ashfold, M. N. R. *J. Chem. Phys.* **1997**, *106*, 6198.
(28) Choi, Y. S. Ph.D. Thesis, University of California at Berkeley, Berkeley, CA, 1991.
(29) Crane, J. C.; Beal, H. P.; Clauberg, H.; Nam, H.; Choi, Y. S.; Moore, C. B.; Stanton, J. F. *J. Mol. Spectrosc.*, in press.
(30) Sumathi, R.; Chandra, A. K. *Chem. Phys.* **1992**, *165*, 257.